Acta Cryst. (1993). A**49**, 56–68

The Videographic Method: a New Procedure for the Simulation and Reconstruction of Real Structures

BY S. H. RAHMAN

Institut für Mineralogie, Universität Hannover, Welfengarten 1, 3000 *Hannover, Germany*

(*Received* 28 *October* 1991; *accepted* 28 *May* 1992)

Abstract

The videographic method is a simulation and reconstruction procedure that uses a statistical mathematical approach and computer graphics to aid the interpretation of scattering (X-ray, electron, neutron) from a disordered crystal. Based on the principles of optical transforms, and in contrast to it, atoms with different scattering power are represented as picture elements (pixels) with different grey levels. Compared with optical transforms, this method has the special advantage that holes of infinitely small radii can simulate different scattering powers in a mask. With the application of a statistical mathematical approach (combination probabilities), various scatterers, *e.g.* atoms, structure variants or domains, can be distributed in a two- or three-dimensional model. A Fourier transformation of the simulated model (diffraction pattern) can be calculated in a few seconds using an array processor and displayed for comparison with experiments. Real-structure image reconstruction can also be performed by amplitude and phase manipulation. As a starting model for a reconstruction, a randomly disordered structure is assumed. Under this assumption, a monotone diffuse background is obtained in the diffraction pattern. The principal idea in a reconstruction of an unknown real structure is that the diffuse regions of a partly ordered structure are a subset of the monotone diffuse background for a random disorder.

1. Introduction

The physical properties of crystalline solids (electrical, mechanical, optical *etc.*) are closely dependent on the chemical-bond type or their atomic structures. The deviation from the periodic arrangement of the atoms in the structure influences the physical properties compared with an ordered crystal.

Examples of disordered crystal structures are point defects, stacking faults, modulations, short-range order and domain formations with different boundaries. The dimension of disordered regions in crystals ranges between the macroscopic and submicroscopic scales.

Besides Bragg reflexions, the diffraction pattern of a disordered crystal shows diffuse components and/or satellite reflexions. The distribution of the satellite reflexions (nonstrictly periodic modulation) or the diffuse components indicates a certain type of disorder.

The influence of crystal-structure disorder on the scattered wave (electron, X-ray and neutron) has led many authors to derive mathematical formulations for the different types of disorder problems (Guinier, 1942; Daniel & Lipson 1944; Jagodzinski, 1949, 1964*a*, *b*, 1987; Kunze, 1959; Korekawa, 1967; Korekawa, Nissen & Philipp, 1970; de Wolff, 1974; Cowley, 1975; Böhm, 1977; Cowley, Cohen, Salamon & Wuensch, 1979; Boysen, Frey & Jagodzinski, 1984).

Parallel to the mathematical developments of the scattering from a disordered crystal, other authors have developed the technique of using optical analogues (Fraunhofer diffraction) to aid the interpretation of X-ray diffractions (Bragg, 1938).

For this purpose, the atoms are replaced by holes in a mask and X-rays by a coherent light source. The deviations from a regular lattice are simulated by varying the positions of the holes. Atoms with different scattering powers are simulated as holes of different radii. One of the earliest applications of disorder problems was carried out by Taylor, Hinde & Lipson (1951). In a second paper, Lipson & Taylor (1951) applied their method successfully to several organic compounds. The mask production was further developed and refined by Harburn (1973) and Harburn, Miller & Welberry, (1974).

When the optical transform method is used to simulate two different scatterers (atoms with different scattering factors), two holes with different radii must be punched and distributed in the mask. The larger hole then represents the atom with the higher scattering power (Amorós & Amorós, 1968; Woolfson, 1970). The main problem is that, when increasing the scattering power by increasing the size of the hole, the angular rate of fall-off will also be increased. This is the reverse of the behaviour of X-ray atomic scattering factors, where usually the higher the atomic number, the more compact it is and therefore the slower is the fall-off. Moreover, the intensities of the Fraunhofer diffraction pattern begin to oscillate more rapidly (Amorós & Amorós, 1968).

The above-mentioned disadvantage of the optical transforms prevents accurate simulation of complex

0108-7673/93/010056-13$06.00

disorder phenomena, especially when domains with different scatterers are distributed in a disordered matrix or a density modulation of the scattering power (Böhm, 1977) is present. For these reasons, most applications of the optical transforms were performed using a unit size for the scatterer (holes or black dots by the photographic technique) (Amorós & Amorós, 1968; Welberry & Galbraith, 1973; Harburn, Taylor & Welberry, 1975). For more details, a review on the applicability of the optical diffraction technique for simulation or reconstruction is given by Rahman (1991).

Nevertheless, the application of the optical Fourier transform to simulate a particular disorder state in crystals can explain some complicated disorder phenomena. This is pointed out by Welberry & Raymond (1980) and Welberry (1985, 1986).

In the present investigation, a new method will be introduced that avoids the above-mentioned disadvantages of optical transforms. Based on a statistical mathematical formulation, the method allows a simulation or a reconstruction of the real structure of a disordered crystal using advanced computer graphics.

The atoms are represented as pixels (picture elements) with different grey levels. A pixel can be considered to be analogous to a hole with an infinitely small radius. The corresponding radius of the airy disk is infinitely large. Pixels with different grey levels but the same size (different scattering powers) behave as point sources that radiate spherical waves when irradiated with 'light'. With use of a pixel-oriented computer-graphic adaptor the structure image can be stored (on video RAM) and displayed on a videographic monitor. The Fourier transform of the 'structure' image stored in memory is performed using parallel computing (with an array processor) in a few seconds and then displayed on a graphic monitor for a comparison with the experimental diffraction pattern. In the following, the method will be referred to as the videographic method (Rahman, 1989, 1991).

The first part of this investigation deals with a mathematical approach to the simulation and reconstruction of disordered structures. This will be accompanied by several specific examples. In two forthcoming papers (Rahman, 1993*a*, *b*), the videographic method is applied to two problems of crystal disorder of different origins, namely the binary compound $AuCu_3$ and the mineral mullite $Al_2[Al_{2+2x}Si_{2-2x}]O_{10-x}$.

2. Experimental

The videographic method is a simulation procedure that uses computer techniques to aid the interpretation of scattering (X-ray, electron, neutron) by a disordered crystal. Therefore, a special hardware component (Rahman, 1989; Rahman & Unser, 1990) and a software package are needed to simulate or reconstruct a certain distribution of scatterers (Rahman, 1991).

The system is based on a personal computer (IBM PC-AT) equipped with two special boards, namely a graphic adaptor and an array processor. Both boards are connected to the PC through the AT-bus interface. The graphic adaptor is able to display and store an image of at least 512×512 pixels with a depth of 8 bits (256 grey levels). The array processor is used to calculate the fast Fourier transform (FFT) of the structure image stored in the video RAM of the graphic adaptor. The transformed (diffraction) image can be immediately displayed on a high-resolution monitor and compared with the experimental diffraction pattern. Both boards communicate with each other through an external port with a high data-transfer rate. A full-frame FFT (512×512) is calculated in 4 s. The transformed image of a disordered-structure model is stored in two arrays. The first array contains the real part and the second contains the imaginary part of a forward Fourier transformation. In this case, allowance is made to manipulate the two parts separately, which is a significant advantage for image reconstruction compared with optical transforms.

The software enables the user to generate pixel graphics with different grey levels easily and rapidly (interactively) to simulate various scatterers (mask). For complicated disorder models, a statistical method (see following section) is developed and programmed to calculate a distribution function for particular disorder types. Three-dimensional real-structure models can also be simulated and implemented for the calculation of short-range-order parameters or the evaluation of any vector correlation (Rahman, 1993*a*, *b*).

3. Mathematical survey

A picture element (pixel) of a two-dimensional image can be described as a function $s(x, y)$ in which s represents the intensity in grey-level quantization and (x, y) are its coordinates. An image with L rows and R columns can be digitally stored or displayed as a two-dimensional array:

$$S(X, Y) = \begin{matrix} s(0,0) & \dots & s(0, R-1) \\ \vdots & \ddots & \vdots \\ s(L-1, 0) & \dots & (L-1, R-1) \end{matrix} . \quad (1)$$

The forward discrete Fourier transformation of an image gives the spatial frequency distribution in the Fourier space with the continuous coordinates u and v,

$$\begin{aligned} Q(u, v) &= \mathcal{F}[S(x, y)] \\ &= (LR)^{-1} \sum_{x=0}^{L-1} \sum_{y=0}^{R-1} S(x, y) \\ &\quad \times \exp[-2\pi i(xu/L + yv/R)]. \end{aligned} \quad (2)$$

A videographic representation of four different structures with various scatterers (pixel intensities) distributed periodically in a two-dimensional lattice are shown in Fig. 1(*a*). The upper left image in Fig. 1(*a*) represents a projection of an ordered $AuCu_3$ structure and the upper right represents an NaCl structure. The lower two images in the same figure show the simulation of two hypothetical complex structures. The corresponding forward Fourier transformations or 'diffraction patterns' (digital transforms) are shown in Fig. 1(*b*).

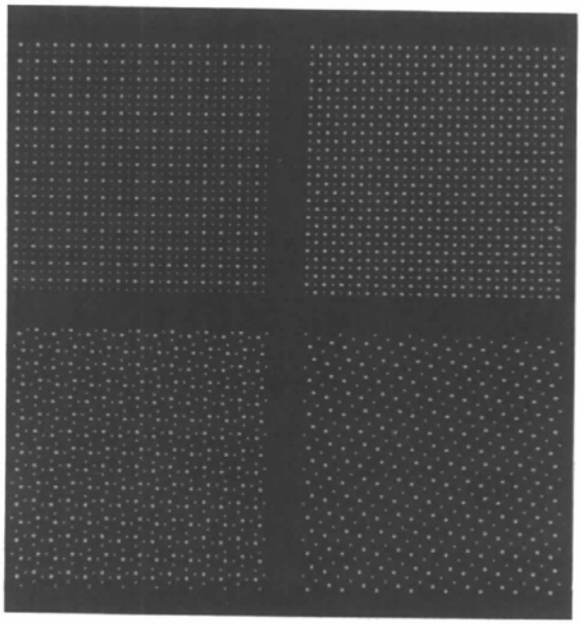

(*a*)

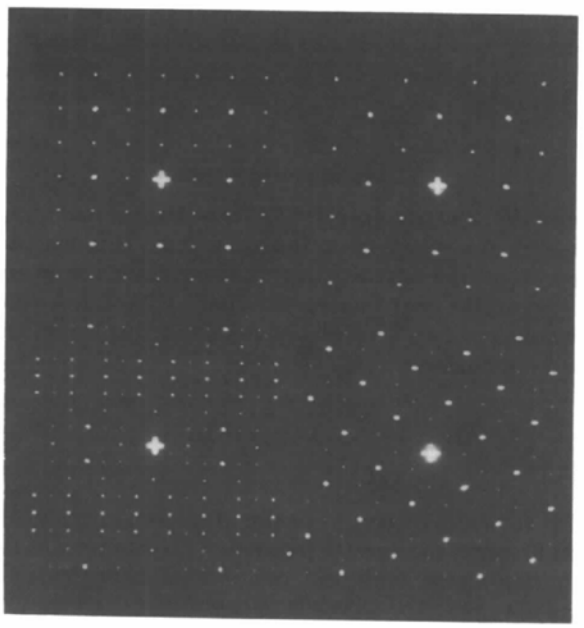

(*b*)

Fig. 1. (*a*) Videographic representation of four two-dimensional ordered structures with different scatterers (pixel intensities). (*b*) Videographic display of the Fourier transformations (FT) of (*a*).

A backward (inverse) Fourier transformation of $Q(u, v)$ reverses the images of Fig. 1(*a*),

$$S(x, y) = \bar{\mathcal{F}}[Q(u, v)] = \sum_{u=0}^{L-1} \sum_{v=0}^{R-1} Q(u, v) \times \exp[2\pi i(xu/L + yv/R)]. \quad (3)$$

$Q(u, v)$ is a complex quantity whose real and imaginary parts are stored separately on the array-processor board. The software allows interactive manipulation of the stored data. In contrast to optical transforms, this provides a valuable facility for image reconstruction.

If a certain type of structure disorder is present, $Q(u, v)$ exhibits, besides the discrete maxima (Bragg reflexions), other more or less diffuse components. The scattering potential $\varphi(x, y)$ of a disordered structure can be expressed (Cowley, 1975) as the sum of the average potential $\langle\varphi(x, y)\rangle$ and the deviation from this average potential $\Delta\varphi(x, y)$,

$$\varphi(x, y) = \langle\varphi(x, y)\rangle + \Delta\varphi(x, y). \quad (4)$$

$\varphi(x, y)$ is equivalent to the electron density in the case of X-ray diffraction or to the scattering potential in electron diffraction. $\varphi(x, y)$ is a real function and can be displayed as pixels with different grey levels.

3.1. *Simulation of the real structures*

An average structure $\langle\varphi(x, y)\rangle$ can be described as a superposition of n possible structure variants or configurations (Rahman, 1991),

$$\langle\varphi(x, y, z)\rangle = N^{-1} \sum_{j=1}^{n} \varphi_j(x, y, z) N_j, \quad (5)$$

where N is the total number of unit cells and N_j is the number of structure variants j.

The number of possible structure variants n from a given average structure can be determined by applying the general crystal chemical rules (interatomic distances, coordination number, bonding energy) during its deconvolution. The real structure consisting of n possible structure variants is given by a certain three-dimensional distribution of N_j cells (in sequence) in the lattice. This can be mathematically described by a distribution function in which all variants need not necessarily be present with the same probability.

To simulate the real structure from its average structure, $\varphi_j(x, y, z)$ must be chosen using a random variable J taking the values j ($j = 1, \ldots, n$) with cer-

Table 1. *Scheme for horizontal and vertical combination probabilities*

Horizontal combinations

	$\varphi_1(x, y)$	$\varphi_2(x, y)$	...	$\varphi_n(x, y)$
$\varphi_1(x, y)$	${}^hW_{11}$	${}^hW_{12}$	...	${}^hW_{1n}$
$\varphi_2(x, y)$	${}^hW_{21}$	${}^hW_{22}$	...	${}^hW_{2n}$
⋮	⋮	⋮	⋱	⋮
$\varphi_n(x, y)$	${}^hW_{n1}$	${}^hW_{n2}$	...	${}^hW_{nn}$

Vertical combinations

	$\varphi_1(x, y)$	$\varphi_2(x, y)$	...	$\varphi_n(x, y)$
$\varphi_1(x, y)$	${}^vW_{11}$	${}^vW_{12}$	...	${}^vW_{1n}$
$\varphi_2(x, y)$	${}^vW_{21}$	${}^vW_{21}$	...	${}^vW_{2n}$
⋮	⋮	⋮	⋱	⋮
$\varphi_n(x, y)$	${}^vW_{n1}$	${}^vW_{n2}$	...	${}^vW_{nn}$

tain probabilities determined by the distribution function of J. The distribution function is defined through the conditional combination probabilities given in Table 1. The probabilities of a combination W_{ji} of two variants $\varphi_j(x, y, z)$ are given in the table for all three translation directions. For a two-dimensional simulation of n possible structure variants, the combination probabilities for the horizontal (${}^hW_{ji}$) and vertical (${}^vW_{ji}$) directions can be tabulated as shown in Table 1.

In the case of a three-dimensional simulation, a third table is needed for the probabilities of combination in the z direction. In this case, a three-sided combination probability is possible. The sum of the probabilities in each row of the tables is equal to 100%. A statistical distribution in the horizontal and vertical directions can be obtained by setting all probabilities to the same value. A forbidden combination between two structure variants can be realized by setting their combination probabilities equal to zero (${}^hW_{ji} = {}^vW_{ji} = 0$).

The real 'structure' image $S(L, M, N)$ resulting from a three-dimensional simulation using combination probabilities W_{ji} of different structure variants or configurations can be expressed as

$$S(L, M, N) = \sum_{l=1}^{L} \sum_{m=1}^{M} \sum_{n=1}^{N} \varphi_{lmn}(J_{lmn}), \qquad (6)$$

where l, m, n are integers, $\varphi_{lmn}(J_{lmn})$ is the structure variant of type J at an lmn position and J_{lmn} is the random variable for an lmn position.

Different distributions of $\varphi_j(x, y, z)$ can be obtained by varying the values of ${}^hW_{ji}$ and ${}^vW_{ji}$. In contrast to other simulation procedures reviewed by Welberry (1985), not only atoms or structure variants (configurations), but also domains with different scatterers or clusters can be distributed within a disordered matrix (Rahman, 1991). Moreover, no restrictions are specified for the magnitude of any correlation vector.

The resulting simulation of (6) can be immediately displayed and stored as a videographic image. To check the result of a simulation, the Fourier transformation of the real-structure image $S(L, M, N)$ must be compared with the experimental diffraction pattern.

The implementation of the above-mentioned statistical method using software to simulate the real structure from the average structure is discussed by Rahman (1991, pp. 17–19) in more detail.

3.2. *Reconstruction of a real structure*

Reconstruction in optical Fourier transforms is a well established technique for image enhancement. For this purpose, a second mask must be produced and placed in the near focal plane of the first lens to filter superimposed noise signals (spatial-frequency or optical filtering). However, this technique is difficult to handle and requires high precision in the mask production. Moreover, the manipulation of both amplitude and phase [(2)] is theoretically not possible (Beeston, Horne & Markham 1972).

Filter operations for the reconstruction are performed in reciprocal space (frequency space). For this purpose, (4) is Fourier transformed and written as

$$\mathcal{F}[\varphi(x, y)] = Q(u, v)_B + \Delta Q(u, v)_d, \qquad (7)$$

$\mathcal{F}[\varphi(x, y)]$ is the Fourier transformation of the real structure, $Q(u, v)_B$ is the scattering amplitude of the Bragg reflexion and $\Delta Q(u, v)_d$ is the scattering amplitude of the diffuse regions.

Besides the Bragg peaks, partly ordered structures show diffuse scattering in their diffraction pattern. Particular detail can be enhanced in an image $S(X, Y)$ by multiplying $Q(u, v)_B$ and $\Delta Q(u, v)_d$ by the transfer functions $G_1(u, v)$ and $G_2(u, v)$, respectively. The value of the transfer functions can be chosen so that either the diffuse regions or the Bragg reflexions are accounted for by a backward Fourier transformation. $G(u, v)$ can also be chosen to transfer only a part of the diffuse region (Rahman, 1989).

The transfer function can be expressed as a convolution (*) between the reciprocal-lattice function $F(u, v)$ and a window function $W(u, v)$,

$$G(u, v) = F(u, v) * W(u, v), \qquad (8)$$

where u and v are continuous coordinates and $F(u, v)$ is the well known reciprocal-lattice delta function,

$$F(u, v) = \sum_h \sum_k \delta(u - ha^*, v - kb^*). \qquad (9)$$

The window function $W(u, v)$ is responsible for the coordinate of the area that is considered for the back transformation.

By application of the above-mentioned reconstruction procedure, a real difference image $S'(x, y)$ is obtained (Rahman & Weichert, 1990):

$$S'(x, y) = \bar{\mathcal{F}}[Q(u, v)_B G_1(u, v) + \Delta Q(u, v)_d G_2(u, v)]. \qquad (10)$$

If a number of different atoms are fully statistically distributed on the same number of permitted sites of a space group (maximum entropy), then $\Delta Q(u, v)_d$ is continuous and decreases monotonically with increasing $(\sin\theta)/\lambda$. $\Delta Q(u, v)_m$ (m for Laue monotonic scattering) has a value at each point that is probably nonzero. Every unit cell is statistically surrounded by other cells with different scatter distributions. The X-ray diffuse intensity for an AB compound with N_A atoms and N_B atoms statistically distributed on the α and β sites is (von Laue, 1960)

$$I_D = Nm_A m_B (f_A - f_B)^2$$
$$m_A = N_A/N, \quad m_B = N_B/N, \quad N = N_A + N_B. \tag{11}$$

A videographic simulation of three statistical distributions generated with randomly chosen start values are shown in Figs. 2(*a*), (*b*), (*c*). The corresponding Fourier transformations are given below in the same figure and show a continuous diffuse background. This means that the atoms do not have any geometrical correlation and their short-range-order parameters (α_{lmn}) are zero. In the case of only partly statistical distributions of various atoms within the unit cell (Fig. 2*d*), the diffuse background is not continuous and its intensity decreases drastically around particular Bragg reflexions.

Substituting (4) into (2) and (7) into (3) results in the following two new equations for the forward and backward Fourier transformations of a partly ordered structure:

$$\langle Q(u, v)\rangle + \Delta Q(u, v) = LR^{-1} \sum_{x=0}^{L-1} \sum_{y=0}^{R-1} [\langle \varphi(x, y)\rangle + \Delta\varphi(x, y)] \exp[-\Omega], \tag{12}$$

$$\langle \varphi(x, y)\rangle + \Delta\varphi(x, y) = \sum_{u=0}^{L-1} \sum_{v=0}^{R-1} [Q(u, v) + \Delta Q(u, v)] \exp[\Omega]. \tag{13}$$

A further substitution in (13), with the right-hand side of (10) taken as a Fourier coefficient and $\Delta Q(u, v)_d$ exchanged with $\Delta Q(u, v)_m$, results in the final equation for the reconstruction of a real structure from a randomly disordered structure,

$$\langle \varphi(x, y)\rangle + \Delta\varphi(x, y) = \sum_{u=0}^{L-1} \sum_{v=0}^{R-1} Q(u, v)_B G_1(u, v) + \Delta Q(u, v)_m G_2(u, v) \exp\Omega,$$
$$\Omega = 2\pi i(xu/L + yv/R). \tag{14}$$

For a reconstruction of a real structure, a starting model in which the atoms are fully statistically distributed must be used (Figs. 2*a*, *b*, *c*). This is, of course, a hypothetical case but it is necessary to obtain a monotonic and relatively high diffuse background $\Delta Q(u, v)_m$ (Rahman, 1992). In this case, the principal idea is that the diffuse region of a partly ordered structure $\Delta Q(u, v)_d$ can be considered as a subset of $\Delta Q(u, v)_m$ [$\Delta Q(u, v)_d \subset \Delta Q(u, v)_m$].

Image reconstruction of a disordered structure can be achieved by selective filtering of certain frequencies from $\Delta Q(u, v)_m$ by means of the transfer function $G_2(u, v)$. The positions of these frequencies can be chosen from a given experimental diffraction pattern of a partly ordered structure. Setting $G_2(u, v) = 0$ for all other frequencies of $\Delta Q(u, v)_m$ and $G_1(u, v) = 1$

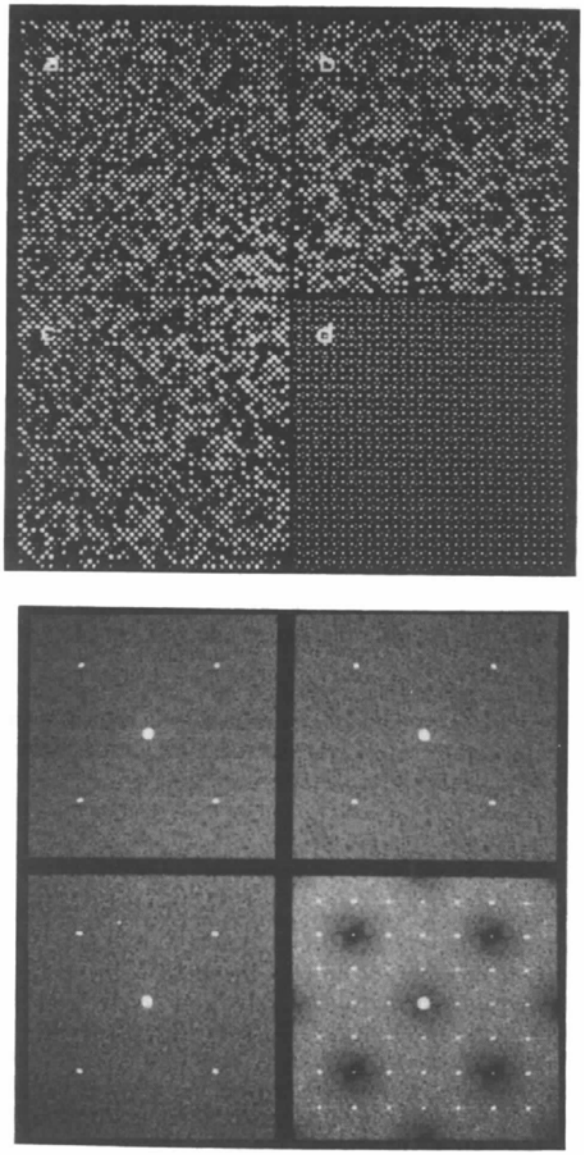

Fig. 2. (*a*), (*b*), (*c*) Videographic simulation of a random distribution of two atoms (scatterers) A and B with different random starts and their Fourier transformations (lower part). (*d*) Random distribution of only the B atoms within the unit cell among five sites (see Fig. 3). FT: lower right corner.

(Bragg reflexion) and performing a backward Fourier transformation [(14)], one can obtain a reconstructed real-structure image (partly ordered structure). All operations during a reconstruction procedure are performed interactively. The start model and the subsequent forward and backward Fourier transformations are controlled by a videographic display.

A videographic representation of the forward Fourier transformation of the reconstructed (diffraction) image can then be compared with the experimental results. When applying (14) to a reconstruction, the software allows the manipulation of amplitude and phase of either $Q(u, v)_B$ or $\Delta Q(u, v)_m$ in different ways, as pointed out in § 4.2.

4. Examples

To illustrate the facilities of the videographic method, a number of examples will be given. The first example considered in §§4.1 and 4.2 demonstrates how the method can be applied to evaluate the real structure from its average structure by either simulation or reconstruction and is discussed in some detail. The other examples, which are discussed briefly, demonstrate the superiority of the method compared with optical transforms when complicated disorder types are present.

4.1. *Simulation of a real structure*

(*a*) *Ordering of a high-temperature phase.* The average structure of a hypothetical AB compound is schematically shown in Fig. 3(*a*). The A atom occupies the (0, 0, 0) site and exhibits a scattering power a factor of two higher than the B atoms. At high temperatures, the B atoms are randomly distributed among five possible positions as shown in Fig. 3(*a*). The decomposition of the average structure into n possible structure variants $\varphi_j(x, y)$ is demonstrated in Figs. 3(*b*) [(5)]. A videographic representation of the five possible structure variants as picture elements (pixels) is given in Fig. 3(*c*). The different scattering power of the A and B atoms is taken into consideration by various grey levels for each pixel representing the atoms. To build up the real structure at various ordering temperatures, a distribution function or tables of values that contain the probabilities of combinations for ${}^hW_{ji}$ and ${}^vW_{ji}$ must be given. A random distribution of the B atoms can be simulated by assigning the same value of 20% to ${}^hW_{ji}$ and ${}^vW_{ji}$. The corresponding combination probabilities for a fully statistical distribution of the five structure variants are given in Table 2.

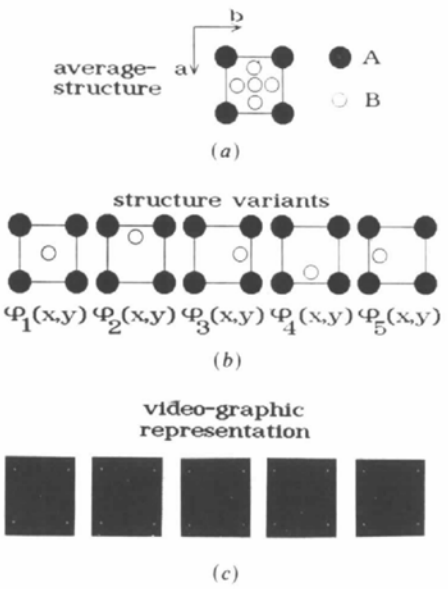

Fig. 3. (*a*) Average structure of an AB compound. The B atoms are randomly distributed among five sites ($f_B = 0.5\, f_A$). (*b*) Five possible structure variants (configurations). (*c*) The videographic representation of (*b*).

Table 2. *Combination probabilities* (%) *for a random distribution of the B atoms* (*see Fig.* 4*a*)

Horizontal combinations						Vertical combinations					
$j \backslash i$	1	2	3	4	5	$j \backslash i$	1	2	3	4	5
1	20	20	20	20	20	1	20	20	20	20	20
2	20	20	20	20	20	2	20	20	20	20	20
3	20	20	20	20	20	3	20	20	20	20	20
4	20	20	20	20	20	4	20	20	20	20	20
5	20	20	20	20	20	5	20	20	20	20	20

From Table 2 it is clear that a structure variant with index $j = 1, \ldots, 5$ (Fig. 3*b*) can be followed in the horizontal and vertical directions by all other variants with the same probability. A videographic simulation after implementing this table in the software is shown on the left-hand side of Fig. 4(*a*). The Fourier transformation (diffraction pattern) of the videographic simulation is shown on the right-hand side of Fig. 4(*a*). Besides the Bragg reflexions, the diffraction pattern shows a diffuse background.

Fig. 4(*a*) represents the real structure of a hypothetical high-temperature phase. If the compound is cooled below T_c, several ordering schemes of the B atoms can be obtained. Such an ordering scheme can be simulated by varying the values of ${}^hW_{ji}$ and ${}^vW_{ji}$ in the combination tables. For the next simulation, the following restrictions (selection rules) are proposed (Fig. 4*b*):

1. The interatomic separations of the B atoms (in neighbouring cells) should be greater than $5a/6$ or $5b/6$.

2. Identical structure variants should not be in direct contact.

If the above-mentioned restrictions are taken into consideration, a new combination table (Table 3) may be set up with the following probabilities:

$${}^hW_{15}, {}^hW_{31}, {}^hW_{35}, {}^vW_{12}, {}^vW_{41}, {}^vW_{42} = 0 \text{ (rule 1)}$$

$${}^hW_{jj}, {}^vW_{jj} = 0 \text{ (rule 2)}.$$

The simulated real structure of the resulting ordering scheme is shown together with its diffraction pattern in Fig. 4(*b*). The diffraction pattern indicates a partial ordering of the structure by a periodic distribution of diffuse regions around the Bragg reflexions.

Another ordering scheme can be obtained by selectively increasing particular combination probabilities and decreasing others as shown in Table 4. The resulting real structure and its Fourier transformation are given in Fig. 4(*c*).

(*b*) *Modulated structures.* A mathematical formulation of X-ray scattering intensities for various types of sine-wave-modulated crystal structures is given by Korekawa (1967). The main types of periodic modulation of a lattice are:

(i) transverse displacement of atoms;
(ii) longitudinal displacement of atoms;
(iii) density modulation or variation of scattering power.

Table 3. *Probabilities* (%) *for the ordering scheme of Fig.* 4(*b*)

Horizontal combinations						Vertical combinations					
$j\backslash i$	1	2	3	4	5	$j\backslash i$	1	2	3	4	5
1	0	33	33	33	0	1	0	0	33	33	33
2	25	0	25	25	25	2	25	0	25	25	25
3	0	50	0	50	0	3	25	25	0	25	25
4	25	25	25	0	25	4	0	0	50	0	50
5	25	25	25	25	0	5	25	25	25	25	0

Table 4. *Probabilities* (%) *for the ordering scheme of Fig.* 4(*c*)

Horizontal combinations						Vertical combinations					
$j\backslash i$	1	2	3	4	5	$j\backslash i$	1	2	3	4	5
1	0	92	4	4	0	1	0	0	4	92	4
2	4	0	88	4	4	2	4	0	4	4	88
3	0	4	0	96	0	3	4	88	0	4	4
4	4	4	4	0	88	4	0	0	96	0	4
5	88	4	4	4	0	5	88	4	4	4	0

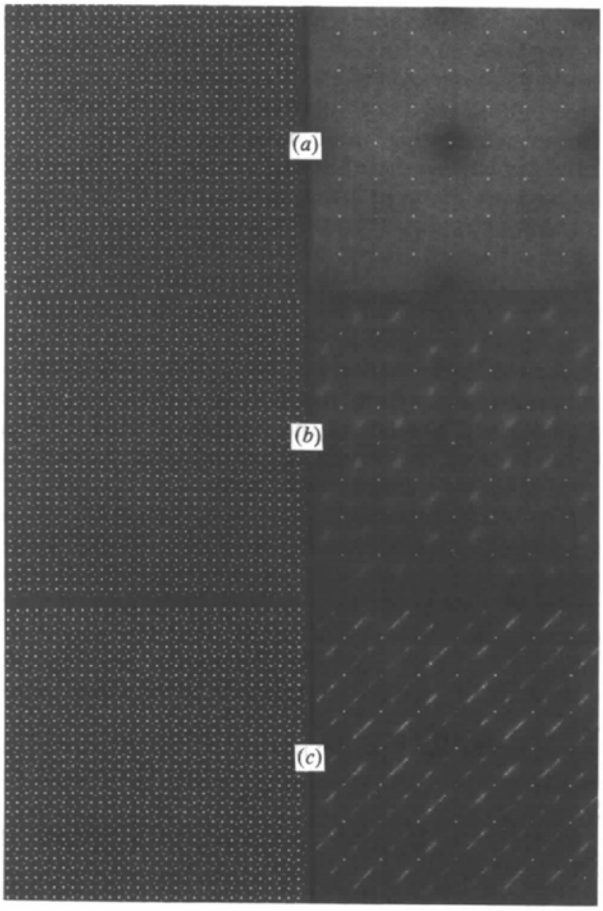

Fig. 4. Videographic simulation of different ordering schemes. (*a*) (Left) Random distribution of the *B* atoms. (Right) Fourier transformation (FT). (*b*) (Left) Partial ordering. (Right) FT. (*c*) (Left) Partial ordering but with different ordering scheme to (*b*). (Right) FT.

Böhm (1977) extended the formulation of Korekawa (1967) to other wave forms and pointed out that the probability of site occupancy is an exceptional case of the density modulation.

A videographic simulation of a transverse displacement of atoms with a superimposed variation of the scattering power is shown in Fig. 5. A scattering-power variation of two parallel sine waves with a phase shift is illustrated in Fig. 6.

The structure simulations of Figs. 5 and 6 were carried out interactively. These represent an idealized model of modulation (for teaching purposes). A more realistic simulation of the variation of the scattering power produced by a site-occupancy distribution of different scatterers is modelled schematically in Fig. 7. The four structure variants differ only in their scattering power. To distribute the structure variants of Fig. 7 to obtain a modulation of the site occupancy, the following selections of the combination probabilities are made:

$$^{h}W_{jj}, {}^{v}W_{jj} = 0 \text{ (diagonal elements)}$$

$$^{h}W_{12}, {}^{h}W_{13}, {}^{h}W_{34}, {}^{h}W_{41} = {}^{v}W_{12}, {}^{v}W_{23}, {}^{v}W_{34}, {}^{v}W_{41} = 96\%$$

and all other probabilities are each set to 2%. The resulting tables are identical for the horizontal and vertical combinations as shown in Table 5. The resulting simulation represents a superstructure due to a quasiperiodic variation of the scattering power of atoms distributed among the same sites. The superstructure is achieved by a preferential selection of the combination probabilities for a sequence of structure variants.

With the preferred combination taken into account, the sequence of the superstructure can be

schematically represented as

1 2 3 4 1 ...
2 3 4 1 2 ...
3 4 1 2 3 ....
4 1 2 3 4 ...
1 2 3 4 1 ...
⋮ ⋮ ⋮ ⋮ ⋮ ⋱

A videographic simulation of this superstructure and its Fourier transformation are given in Fig. 8. The simulation shows planes with equal phase shifts running parallel to [$\bar{1}$10] (Korekawa, 1967).

(*c*) *Antiphase domains.* Many order/disorder phase transitions are accompanied by a domain formation in a crystal. In some compounds (intermetallic phases), the domains are in an antiphase relationship

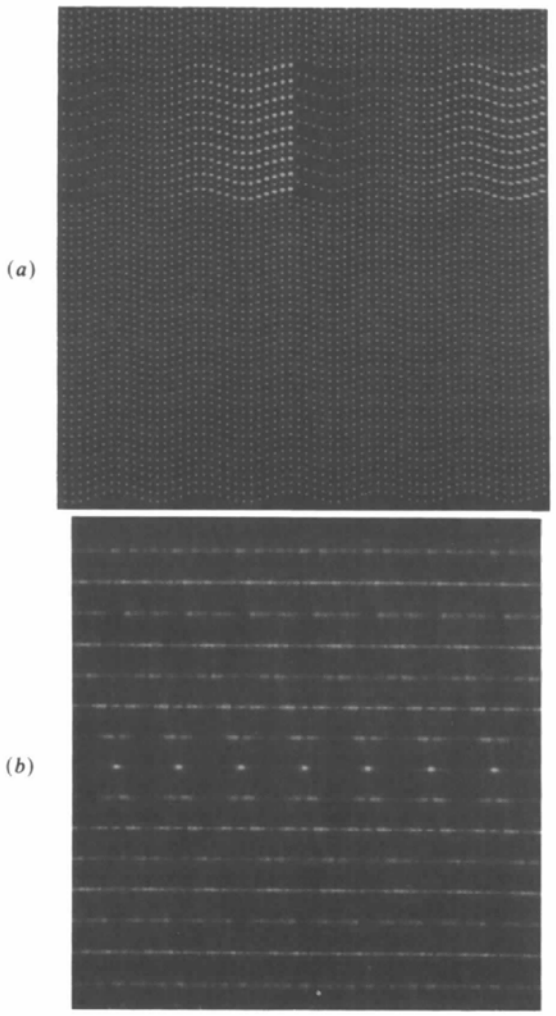

Fig. 5. (*a*) Videographic simulation of a transverse wave superimposed on a density wave. (*b*) FT.

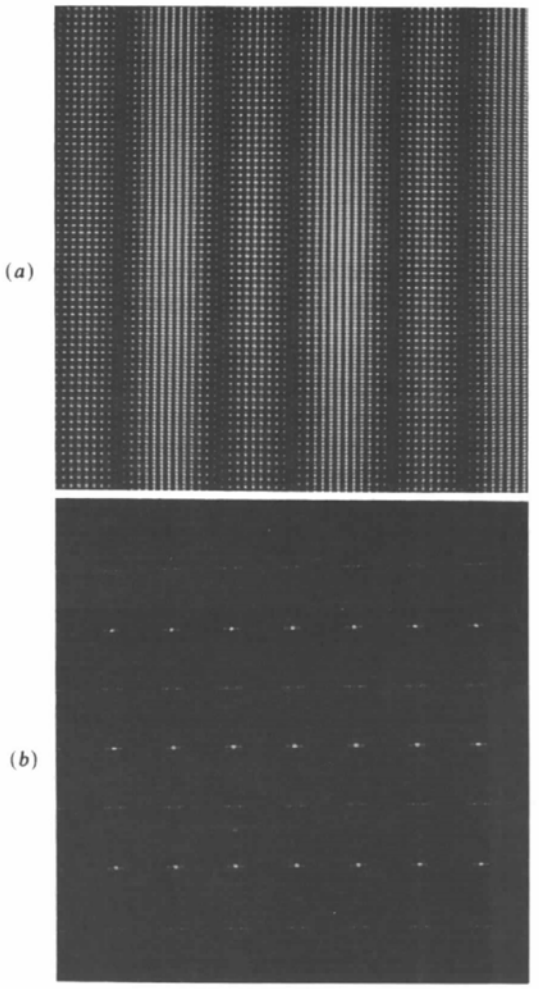

Fig. 6. (*a*) Videographic simulation of two parallel density waves with $\Phi_{D1,1} = -M_1/4$ after Korekawa (1967). (*b*) FT.

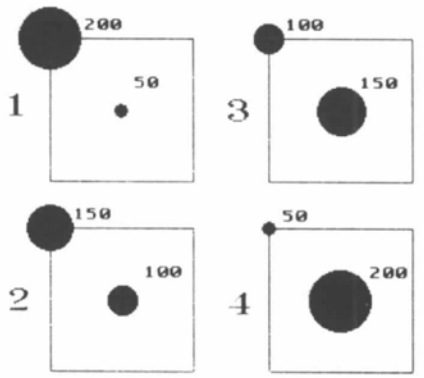

Fig. 7. Structure variants for the videographic simulation of a modulation by varying the scattering power. The radius of the black circle is proportional to the scattering power or the pixel intensity, which varies between 50 and 200.

Table 5. *Combination probabilities* (%) *of Fig.* 8

Horizontal combinations

$j \backslash i$	1	2	3	4
1	0	96	2	2
2	2	0	96	2
3	2	2	0	96
4	96	2	2	0

Vertical combinations

$j \backslash i$	1	2	3	4
1	0	96	2	2
2	2	0	96	2
3	2	2	0	96
4	96	2	2	0

and are distributed in a disordered matrix (Cowley, 1965). The domain size is dependent on heat treatment.

Table 6 shows different types of two-dimensional lattices and unit-cell parameters for the matrix and antiphase domains. The videographic simulations of the antiphase cluster of the five types given in Table 6 are shown with their Fourier transformations in Fig. 9. In all simulations the antiphase boundary runs parallel to [010]. The diffraction pattern of the first four simulations shows weak and diffuse superstructure reflexions. Their positions in the diffraction pattern are in accordance with the systematic presence of the antiphase-domain lattice type. Normally, such reflexions split into doublets according to the interference function (Raether, 1952). The splitting direction is perpendicular to the antiphase boundaries. A complete discussion of the relationship between domain sizes and their distribution in a matrix on the superstructure reflex shape is given by Rahman (1991).

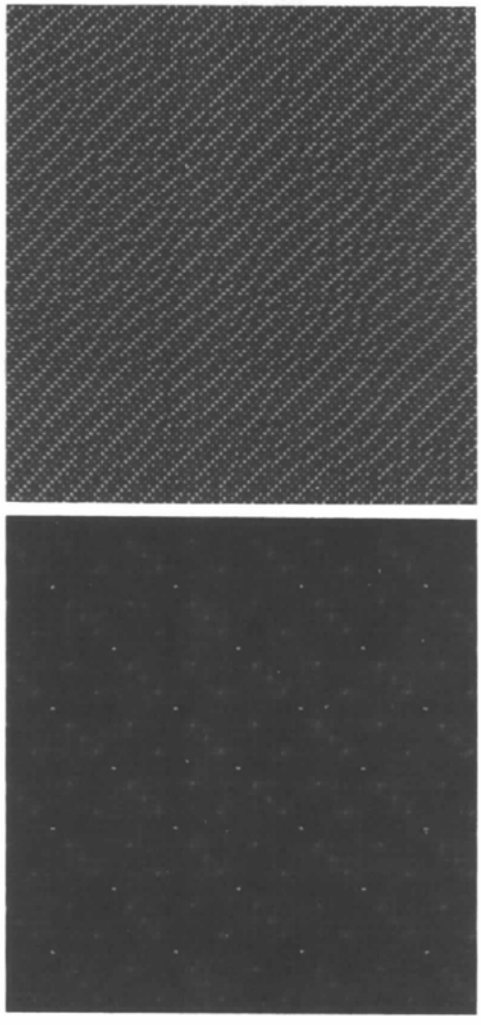

Fig. 8. (*a*) Simulation of density waves with the same phase shift parallel to [110]. (*b*) FT.

Table 6. *Lattice type and unit-cell parameters of matrix and antiphase domains*

No. (Fig. 9)	Matrix Lattice	Matrix Cell parameters	Antiphase domain Lattice	Antiphase domain Cell parameters
1	*p*	*a*, *b*	*p*	2*a*, 2*b*
2	*p*	*a*, *b*	*c*	2*a*, 2*b*
3	*c*	*a*, *b*	*p*	*a*, *b*
4	*c*	*a*, *b*	*c*	2*a*, 2*b*
5	*c*	*a*, *b*	*c*	*a*, *b*

The contribution of the (precipitate) antiphase domains to the diffraction pattern in Fig. 9, example 5 is not visible because they are superimposed on the Bragg peak of the matrix. However, depending on the domain size and accumulation, the Bragg peak could have a diffuse corona.

4.2. *Reconstruction of a real structure*

The reconstruction of a real structure is based on the idea that the part of a diffuse region in the reciprocal space of such a structure is a subset of the monotone diffuse background of a randomly disordered structure $[\Delta Q(u, v)_d \subset \Delta Q(u, v)_m]$. Consequently, the atoms of starting model for a reconstruction must be randomly distributed to obtain a monotone continuous diffuse background in its diffraction pattern (forward Fourier transformation, Rahman 1992) (Figs. 2*a*, *b*, *c*). The diffuse background is a complex quantity $(A+iB)$, whereas the transfer function $G_2(u, v)>0$ is a real quantity. If $G_2(u, v)$ is multiplied by $(A+iB)$, only an amplitude change is obtained. Amplitude and phase changes can be achieved when the multiplication in (14) is modified to $G_{2a}(u, v)A+G_{2b}(u, v)iB$, with use of a separate window function. The indices *a* and *b* denote the real and imaginary parts, respectively. The abovementioned multiplication procedure for the manipulation of amplitude and phase by a reconstruction is implemented in the software and can be performed interactively whilst viewing the image on a high-resolution monitor.

(*a*) *Short-range order and the formations of antiphase domains.* HRTEM investigations of order/disorder phase transitions show that the degree of diffusivity of the superstructure reflexions is dependent on the antiphase domain size (Schleiter, Kroll

& Rahman 1989). With increasing temperature, the domain sizes decrease and they are distributed in a disordered matrix.

For the reconstruction of such real-structure images, a starting model with two different scatterers (atoms) is chosen. The atoms are randomly distributed at the corners of a primitive cubic cell. The model and the corresponding forward Fourier transformation are shown respectively on the left-hand and right-hand sides of Fig. 10(*a*). To reconstruct short-range order with antiphase domain formations, a circular pixel group is selected at the superlattice reflexion positions (diffuse superlattice reflexion). This procedure is demonstrated in Fig. 10(*b*) for two

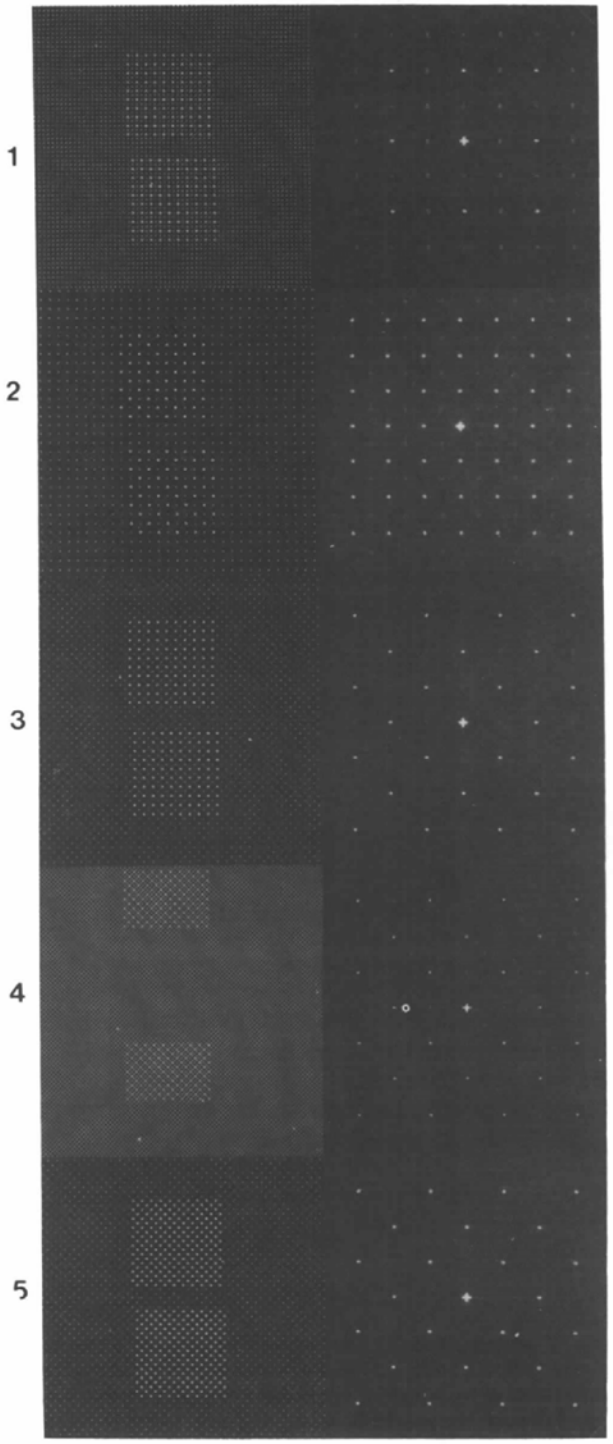

Fig. 9. (Left) Videographic simulation of antiphase domain clusters in a matrix (see Table 6). (Right) FT's.

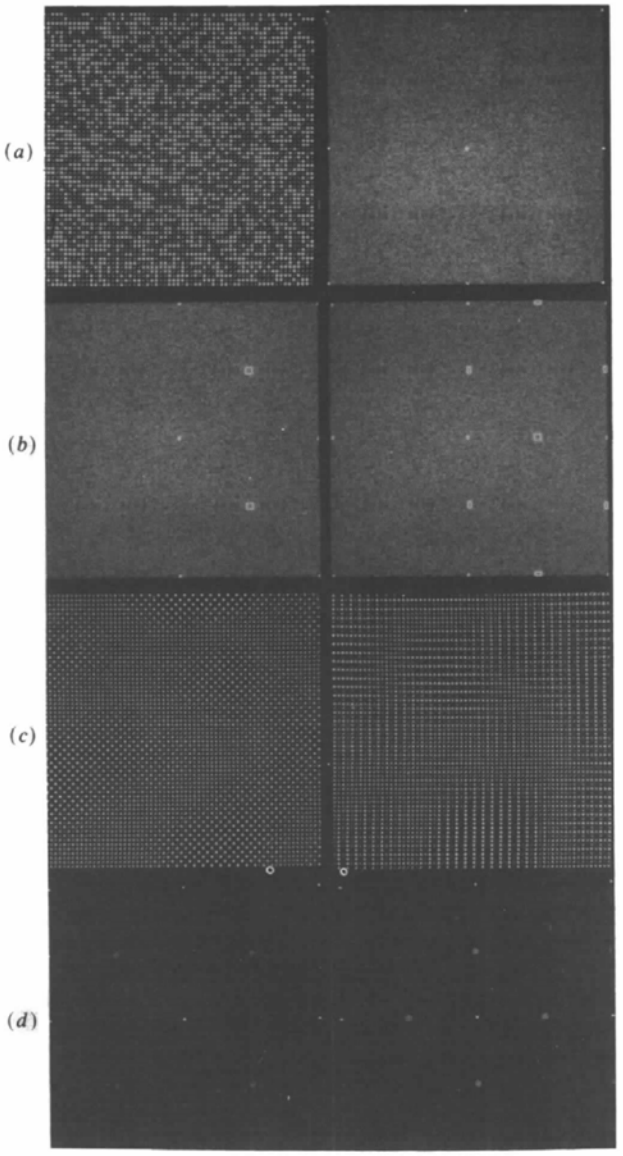

Fig. 10. (*a*) (Left) Random distribution of two scatterers (starting model). (Right) FT. (*b*) Selected diffuse regions for two reconstructions with different positions of the superlattice reflexions. The positions are marked only on one half of the diffraction pattern. (*c*) (Left) Reconstructed image showing antiphase domains with boundaries parallel to [110] and [1$\bar{1}$0]. (Right) Antiphase domain boundary parallel to [1$\bar{0}$0] and [010]. (*d*) FT's from reconstructed images.

reconstructions. The selected areas from the diffuse background are marked by white squares (only in one half of the diffraction patterns). In the first example, they are positioned at the centre of the absent 110 and $\bar{1}10$ reflexions [Fig. 10(*b*), left] and, in the second example, at the centre of the 100 and 010 reflexions [Fig. 10(*b*), right]. The backward Fourier transformations are performed by selecting $G_2(u, v) = 10$ and $G_1(u, v) = 1$. The reconstructed structure images for the two examples are given in Fig. 10(*c*). Both images show a distribution of antiphase domains in a disordered matrix. In the first case [Fig. 10(*c*), left], the antiphase domain boundaries run parallel to [110] and [$1\bar{1}0$]. In the second case [Fig. 10(*c*) right], they run parallel to [100] and [010]. To confirm the results of the reconstruction

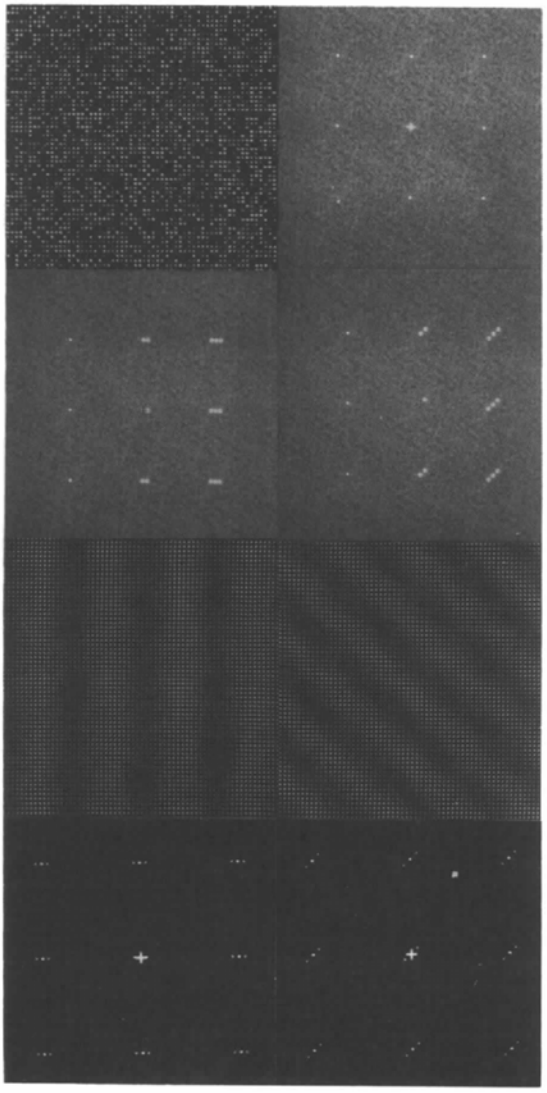

Fig. 11. (*a*) (Left) Starting model. (Right) FT. (*b*) Selected positions of the satellite reflexions for two modulation directions. (*c*) Reconstructed images. (*d*) FT's of the reconstructed images.

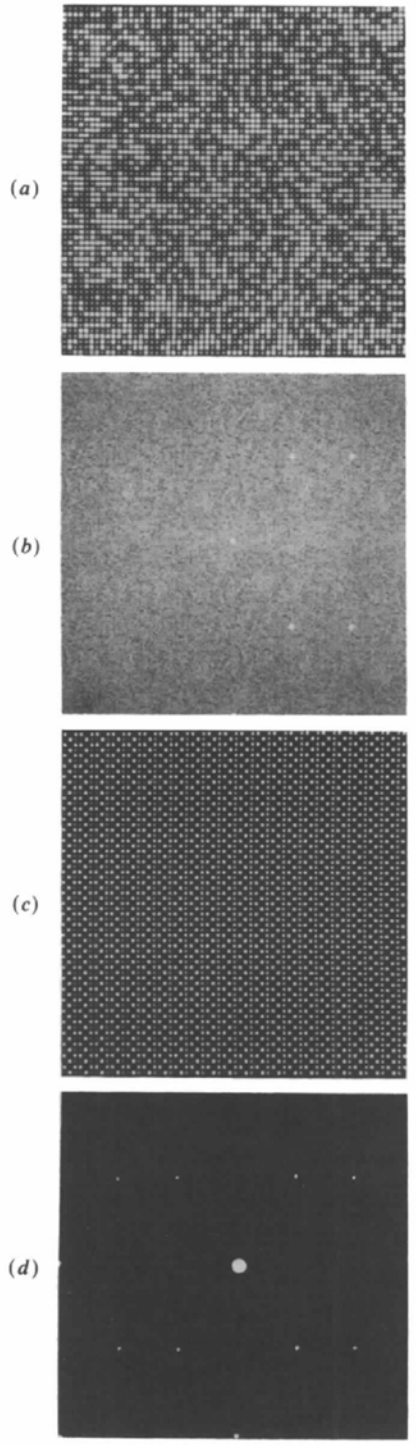

Fig. 12. (*a*) Starting model. (*b*) Fourier transform of the start model with marked satellite positions. (*c*) Reconstructed image showing variation of intensities in horizontal rows. (*d*) Forward Fourier transformation showing the satellite reflexions around the absent 110 reflexion group.

procedure, the images of Fig. 10(*c*) are Fourier transformed as shown in Fig. 10(*d*). The positions of the diffuse superlattice reflexions are fully in accordance with the simulation given in Fig. 9 for different antiphase-domain types.

(*b*) *Density modulation.* For the reconstruction of a sine-wave modulation of the scattering power, an identical start model as in the foregoing example is used (Fig. 11*a*). The positions of the satellite reflexions for two different modulation directions are selected symmetrically with respect to the Bragg reflexions as shown in Fig. 11(*b*) (Korekawa, 1967). A good match for a density modulation is achieved by assigning values 16 and 1 to $G_2(u, v)$ and $G_1(u, v)$, respectively. The reconstructed real-structure images are shown in Fig. 11(*c*) for a modulation direction parallel to [010] [Fig. 11(*c*), left] and [$\bar{1}$10] [Fig. 11(*c*), right]. A forward Fourier transformation of the reconstructed images results in diffraction patterns (Fig. 11*d*) indicating the type of modulation as reported by Korekawa (1967).

(*c*) *Modulation through probability variation of the site occupancy.* In the foregoing example, the satellite reflexions are positioned symmetrically with respect to a present Bragg reflexion. In several other cases (mullite $Al_2[Al_{2+2x}Si_{2-2x}]O_{10-x}$; Guse & Saalfeld, 1976; Cameron, 1977), the satellite reflexions are positioned symmetrically with respect to an absent Bragg reflexion. An example of such a case is reconstructed in Fig. 12. The regions for the reconstruction are positioned on the left- and right-hand sides of the absent 110 reflexion groups (Fig. 12*b*). From the reconstructed image (Fig. 12*c*), it can easily be seen that the intensity in a horizontal row varies smoothly. This observation can be interpreted (Böhm, 1977) as a variation of the probability of a site occupancy, which represents a special case of density modulation (Rahman & Weichert, 1990).

5. Concluding remarks

The examples discussed in §4 demonstrate the wide application range of the videographic method. By representing the real structure as a videographic image, the whole content of a structure configuration can be displayed as picture elements with different grey levels. By this procedure, complicated disorder phenomena in which more than one disorder mechanism is present are able to be investigated.

Both simulation and reconstruction can be applied to discover a real-structure configuration. Also, a combination of both methods is useful. Other interesting features include a facility to manipulate phase and amplitude by a reconstruction and the simulation of three-dimensional models using three-sided combination probabilities (Rahman, 1993*a*, *b*). From such three-dimensional simulations, vector correlations can be estimated and compared with experimental results.

References

AMORÓS, J. L. & AMORÓS, M. (1968). *Molecular Crystals: Their Transforms and Diffuse Scattering.* New York, London, Sydney: John Wiley.

BEESTON, B. E. P., HORNE, R. W. & MARKHAM, R. (1972). *Electron Diffraction and Optical Diffraction Techniques.* Amsterdam, London, New York: North-Holland/Elsevier.

BÖHM, H. (1977). Habilitationsschrift, Westfälischen Wilhelms-Univ., Münster, Germany.

BOYSEN, H., FREY, F. & JAGODZINSKI, H. (1984). *The Rigaku Journal*, **1**, No. 2, pp. 3-14.

BRAGG, W. L. (1938). *Nature (London)*, **143**, 678-680.

CAMERON, W. E. (1977). *Am. Mineral.* **62**, 747-755.

COWLEY, J. M. (1965). *Phys. Rev. A*, **138**, 1384-1389.

COWLEY, J. M. (1975). *Diffraction Physics.* Amsterdam: North-Holland.

COWLEY, J. M., COHEN, J. B., SALAMON, M. B. & WUENSCH, B. J. (1979). *Modulated Structures, AIP Conf. Proc.* Vol. 53. New York: American Institute of Physics.

DANIEL, V. & LIPSON, H. (1944). *Proc. R. Soc. London Ser. A*, **128**, 378-387.

GUINIER, A. (1942). *J. Phys. (Paris)*, **8**, 124-134.

GUSE, W. & SAALFELD, H. (1976). *Z. Kristallogr.* **143**, 177-187.

HARBURN, G. (1973). *Optical Fourier Synthesis in Optical Transforms*, edited by H. S. LIPSON. New York: Academic Press.

HARBURN, G., MILLER, J. S. & WELBERRY, T. R. (1974). *J. Appl. Cryst.* **7**, 36-38.

HARBURN, G., TAYLOR, C. T. & WELBERRY, T. R. (1975). *Atlas of Optical Transforms.* London: Bell & Hyman.

JAGODZINSKI, H. (1949). *Acta Cryst.* **2**, 201-207.

JAGODZINSKI, H. (1964*a*). *Advances in Structure Research by Diffraction Methods*, Vol. I, edited by R. BRILL. Braunschweig: Friedrich Vieweg und Sohn.

JAGODZINSKI, H. (1964*b*). *Advanced Methods of Crystallography*, edited by G. N. RAMACHANDRAN. London, New York: Academic Press.

JAGODZINSKI, H. (1987). *Prog. Cryst. Growth Charact. Mater.* **114**, 47-102.

KOREKAWA, M. (1967). Habilitationsschrift, Ludwig-Maxmilians-Univ., München, Germany.

KOREKAWA, M., NISSEN, H.-U. & PHILIPP, D. (1970). *Z. Kristallogr.* **131**, 418-436.

KUNZE, G. (1959). *Z. Kristallogr.* **111**, 190-221.

LAUE, M. VON (1960). *Röntgenstrahl-Interferenzen.* Frankfurt am Main: Akademie Verlagsgesellschaft.

LIPSON, H. & TAYLOR, C. A. (1951). *Acta Cryst.* **4**, 458-462.

RAETHER, H. (1952). *Z. Angew. Phys.* **4**, 53-59.

RAHMAN, S. H. (1989). *Z. Kristallogr.* **186**, 116-118.

RAHMAN, S. H. (1991). Habilitationsschrift, Univ. Hannover, Germany.

RAHMAN, S. H. (1992). Xth European Congress on Electron Microscopy, Granada, Spain, September 1992, General Suppl. In the press.

RAHMAN, S. H. (1993*a*). *Acta Cryst.* **A49**, 68-79.

RAHMAN, S. H. (1993*b*). In preparation.

RAHMAN, S. H. & UNSER, D. (1990). *Design Elektron.* **11**, 70-73.

RAHMAN, S. H. & WEICHERT, H.-T. (1990). *Acta Cryst.* **B46**, 139-149.

SCHLEITER, M., KROLL, H. & RAHMAN, S. H. (1989). *Z. Kristallogr.* **186**, 259-261.

TAYLOR, C. A., HINDE, R. M. & LIPSON, H. (1951). *Acta Cryst.* **4**, 262-266.

WELBERRY, T. R. (1985). *Rep. Prog. Phys.* **48**, 1543-1593.

WELBERRY, T. R. (1986). *J. Appl. Cryst.* **19**, 382-389.
WELBERRY, T. R. & GALBRAITH, R. (1973). *J. Appl. Cryst.* **6**, 87-96.
WELBERRY, T. R. & RAYMOND, D. G. (1980). *J. Appl. Cryst.* **13**, 244-251.
WOLFF, P. M. DE (1974). *Acta Cryst.* A**30**, 777-785.
WOOLFSON, M. M. (1970). *X-ray Crystallography*. Cambridge Univ. Press.

Acta Cryst. (1993). A**49**, 68-79

The Local Domain Configuration in Partially Ordered $AuCu_3$

BY S. H. RAHMAN

Institut für Mineralogie, Universität Hannover, Welfengarten 1, 3000 *Hannover, Germany*

(*Received* 28 *November* 1991; *accepted* 27 *May* 1992)

Abstract

If the videographic simulation method is applied, the real structure configuration of the domains formed in a partially ordered $AuCu_3$ crystal is established. Each domain is formed by four ordered $AuCu_3$ blocks. The blocks are interconnected crosswise by two different domain boundaries, namely the preferred antiphase domain boundary and the new domain interface structure (I cells of the composition Au_2Cu_6). Six symmetry-related domains exist with the above-mentioned domain structure. An $AuCu_3$ crystal that shows the characteristic two- and four-fold splitting of the superlattice reflexions in its diffraction pattern (of partial order) contains at least two such domain configurations at 90° relative to each other. A two- and three-dimensional simulation using different combination probabilities and structure variants allows a quantitative description of the real configuration of the $AuCu_3$ structure at different temperatures to be made.

1. Introduction

Many X-ray investigations have been made to study the order/disorder transitions of binary alloys. These include the interpretation of the diffuse scattering from disordered crystals. For this purpose, simple cubic AB and AB_3 structures (intermetallic phases) were used. A classic example is the copper-gold alloy $AuCu_3$. This compound exhibits, compared to other intermetallic compounds *e.g.* β-CuZn, a relatively low critical temperature ($T_c = 663$ K) and a large difference in scattering powers ($f_{Au} = 2.8 f_{Cu}$). The above-mentioned properties make $AuCu_3$ an interesting phase for many investigations in the field of short- and long-range-order phenomena (Sykes & Jones, 1936; Jones & Sykes, 1938; Cowley, 1950; Chapman, 1956; Wilson, 1962; Guinier, 1963; Warren, 1968).

$AuCu_3$ exhibits a simple cubic ordered structure at room temperature ($a = 3.72$ Å, see Fig. 1*a*). With increasing temperature the Au atoms can exchange their sites with the Cu atoms (Fig. 1). The intensities of the Bragg reflexions with mixed indices (superlattice reflexions) decrease with increasing temperature. At the critical temperature, long-range order vanishes ($S = 0$) and the intensities of the superlattice reflexions (I_{100}, I_{110}, I_{300} *etc.*) are almost zero. Above T_c, only short-range-order phenomena are present (Edmunds, Hinde & Lipson, 1947; Wilson, 1947; Cowley, 1950; Edmunds & Hinde, 1952; Chapman, 1956).

Around the positions of the superlattice reflexions a diffuse background with a characteristic distribution (shape) is present (Fig. 2*c*) (Wilson, 1947; Cowley, 1950).

An $AuCu_3$ crystal cooled from about 873 K to a temperature below T_c (about 373 K) gives rise to a fine structure of the superlattice reflexions (of partial order) as schematically shown in Fig. 2(*b*) (Raether, 1952; Yamaguchi, Watanabe & Ogawa, 1961; Sinclair & Thomas, 1975). Inspection of the a^*b^* plane reveals that superlattice reflexions with h and k mixed

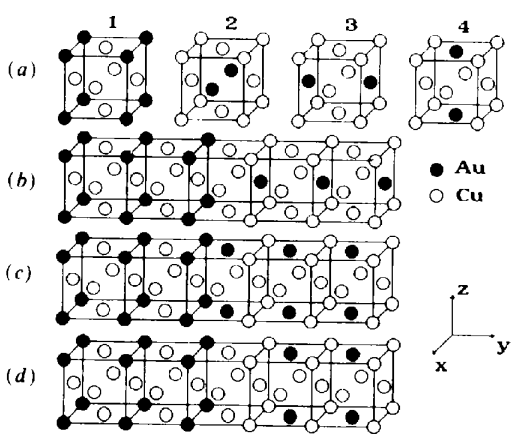

Fig. 1. (*a*) $AuCu_3$ structure variants. (*b*) Antiphase domain boundary of the favoured type. (*c*), (*d*) Antiphase domain boundary of nonfavoured types.

0108-7673/93/010068-12$06.00